Journal of Civil Engineering and Architecture 12 (2018) 323-334
doi: 10.17265/1934-7359/2018.05.001

A Virtual Work Approach to Modeling the Nonlinear Behavior of Steel Frames

Barry T. Rosson

Department of Civil, Environmental and Geomatics Engineering, Florida Atlantic University, Boca Raton, FL 33431, USA

Abstract: The stiffness reduction is studied in detail of compact W-Shapes (wide-flange steel shapes) that results from yielding of the cross-section due to uniaxial bending and axial compression. Three-dimensional m-p-τ surface plots developed from detailed fiber element models of a W8x31 are used to develop a generalized material model for direct implementation in the virtual work method. A portal steel frame is used to illustrate the virtual work method with the nonlinear material model in a first-order, inelastic analysis implementation and in a second-order, inelastic analysis condition. The nonlinear modeling capabilities of MASTAN2 are used to verify the accuracy of the virtual work results and are found to be in very close agreement.

Key words: Nonlinear analysis, steel beam-columns, stiffness reduction, material model, virtual work.

1. Introduction

The in-plane behavior of steel frames with compact doubly-symmetric beam-columns that are subjected to major or minor axis bending has been shown to exhibit significant differences in their response based on plastic hinge and plastic zone analyses [1, 2]. Frames of this type with little to no redundancy can be very sensitive to the refinement of the inelastic analysis procedure employed [3, 4]. Recent research has focused on developing improved empirical relationships to account for the reduction in stiffness that occurs due to yielding of the beam-column's cross-section [5-7]). The objective of this paper is to present the findings from a detailed fiber element model investigation of the stiffness reduction that develops as a result of yielding in the flanges and web over the full range of moment and axial load combinations from initial yield to the fully plastic condition. Considering major axis or minor axis bending under axial compression conditions, analytical expressions are presented to determine the moment and axial load combinations at the initial onset of yielding and when the section becomes fully plastic.

Closed-form equations are presented that provide a straightforward and relatively easy to use material model when conducting a nonlinear analysis of planar steel frames with compact W-Shapes (wide-flange steel shapes) using the virtual work method. Expressions for the stiffness reduction over the length of the member in a virtual work application with linear moment variation are also presented. The material model can accommodate any W-Shape and assumed maximum value of residual stress.

Discussion is provided on how the equations can be used as tangent modulus values in the nonlinear analysis program MASTAN2 [8]. The use of the material model is first demonstrated for a steel portal frame with first-order, inelastic response behavior. The virtual work method is then extended to consider second-order effects. The concluding section combines the findings from the previous section to consider the virtual work and MASTAN2 models of a steel frame with second-order, inelastic response behavior.

2. Modeling Inelastic W-Shape Behavior

A nonlinear analysis requires a series of linear analyses with load increments up to the fully applied

Corresponding author: Barry T. Rosson, professor, research field: modeling nonlinear structural behavior.

load condition or to a lower magnitude if an instability occurs prior to full load application. By introducing increments of load ΔH and virtual load ΔQ, an expression for the displacement at *c* due to the load H can be found for the frame in Fig. 1 with inelastic material behavior. Throughout this load increment condition, the material behavior and deformations of the frame are held constant at the conditions immediately prior to ΔH and ΔQ being applied.

Using δ_{cb} to represent the increment of displacement at *c* due to the load ΔH at *b*, the virtual work relationship is

$$\Delta Q \delta_{cb} = \sum_{k=1}^{4} \int_0^{L_k} \frac{\Delta M_k^H \Delta M_k^Q}{EI_k^*} dz \qquad (1)$$

where EI_k^* is the stiffness condition in member *k* immediately prior to the next application of load ΔH. The integral expression can be simplified for an individual member *k* by considering the moments $\Delta M^{\mathrm{H}}(z)$ and $\Delta M^{\mathrm{Q}}(z)$ to be continuous functions over the length L_k. Since ΔQ is a concentrated force, $\Delta M^{Q}(z)$ will always be a linear function $(a + bz)$ such that

$$\int_0^{L_k} \frac{\Delta M^H(z)}{EI_k^*} \Delta M^Q(z) dz = \int_0^{L_k} \frac{\Delta M^H(z)}{EI_k^*} (a + bz) dz \qquad (2)$$

where $\Delta M^{H}(z)/EI_k^*$ is the curvature equation due to the load ΔH, and $\Delta M^{\mathrm{Q}}(z)$ is the moment equation due to the virtual load ΔQ. Eq. (2) can be written in the following form

$$a \int_0^{L_k} \frac{\Delta M^H(z)}{EI_k^*} dz + b \int_0^{L_k} \frac{\Delta M^H(z)}{EI_k^*} z\, dz = A_k^*(a + b\bar{z}) = A_k^*(\Delta \bar{M}^Q) \qquad (3)$$

The incremental displacement at any point *j* can be determined using the following generalized form of the virtual work equation

$$\delta_j = \sum_{k=1}^{n} A_k^* (\Delta \bar{M}_k^Q) \qquad (4)$$

where A_k^* is the incremental area of the curvature diagram with stiffness that varies over the member length L_k, and $\Delta \bar{M}_k^Q$ is the moment at the centroid of each area due to ΔQ = 1 at *j*.

Consider the steel frame in Fig. 1 to have compact W-Shape sections with elastic, perfectly plastic material properties as depicted in Fig. 2. Provided the load H is large enough to produce an inelastic material response, Eq. (4) can be used to find the lateral displacement at any point *j*.

The moment condition between the yield moment M_y and the plastic moment M_p is the elasto-plastic moment M_{ep}. At this magnitude of moment, the cross-section has a specific value of reduced flexural stiffness EI_{ep}. Recognizing that plane sections remain plane after bending, even after a portion of the cross-section has yielded, the curvature equation is given as

$$\phi = \frac{M_{ep}}{EI_{ep}} = \frac{M_{ep}}{\tau EI} \qquad (5)$$

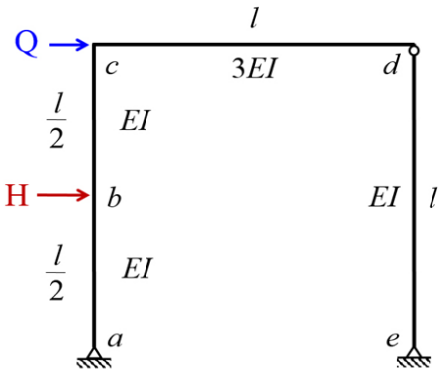

Fig. 1 Steel frame with loads H and Q.

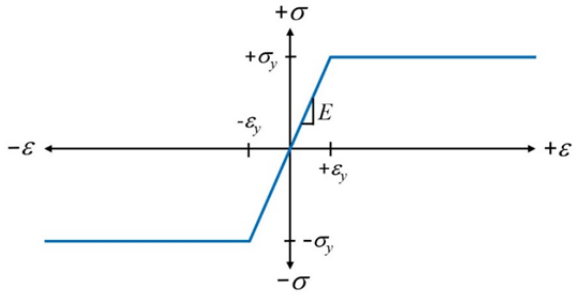

Fig. 2 Elastic, perfectly-plastic material.

The bending moment M_e is defined to be the moment that would exist if the cross-section had not yielded and maintained its full stiffness EI. At this condition of moment and stiffness, the curvature is defined to be the same as the actual condition of moment M_{ep} with reduced stiffness EI_{ep}.

$$\phi = \frac{M_e}{EI} = \frac{M_{ep}}{EI_{ep}} \tag{6}$$

From Eqs. (5) and (6), the relationship for τ in terms of the moments M_{ep} and M_e is given as

$$\tau = \frac{M_{ep}}{M_e} \tag{7}$$

The stiffness reduction that results from yielding of the cross-section due to bending up to the plastic moment M_p and axial compression up to the yield load P_y was studied in detail for W-Shapes with an ECCS (European Convention for Constructional Steelwork) [9] residual stress pattern as depicted in Fig. 3 [10]. For a given normalized moment m (M/M_p), normalized axial load p(P/P_y), and residual stress ratio c_r(σ_r/σ_y), the stiffness reduction was carefully assessed using a detailed fiber element model of a W8x31 [11] with c_r = 0.3.

A computer program was developed to accommodate a specified number of rows and columns of fiber elements in each flange and the web. The angle and location of linear strain distribution were varied in specified increments from zero to specified maximums in order to capture the m and p conditions at 0.01 increments to at least three significant digits of accuracy.

At each condition of strain distribution, the stresses in all of the fiber elements were used to calculate the corresponding moment and axial load condition. When yielding occurred, the M_{ep} and M_e conditions were used to evaluate the corresponding stiffness reduction using Eq. (7). The W-Shape model used 2,046 elements over the cross-section (400 fiber elements in each flange and 1,246 fiber elements in the web). This level of discretization was found to be necessary to develop the smooth m-p-τ surface plot in Fig. 4 [10]. Using the m and p results with increments of 0.01, over 7,000 data points were used to produce the three-dimensional surface plots (m and p conditions of τ = 0 outside of the boundary were excluded).

For a given residual stress ratio c_r and axial compression load condition p, the maximum moment m_1 at which τ = 1 is maintained is given as

$$m_1 = \frac{S_y}{Z_y}(1 - c_r - p) \tag{8}$$

$$m_1 = \frac{S_x}{Z_x}(1 - c_r - p) \tag{9}$$

where S_y is the minor axis elastic section modulus, Z_y is the minor axis plastic section modulus, S_x is the major axis elastic section modulus, and Z_x is the major axis plastic section modulus.

Two equations are needed to determine the m and p conditions when τ = 0 for both the minor axis and major axis bending conditions. For a given p condition, the minor axis bending moment $m_0$at which τ = 0 is given as

$$m_0 = 1 - \frac{p^2(2+\lambda)^2}{(2+\lambda\lambda_o)(2+\lambda_1)} \tag{10}$$

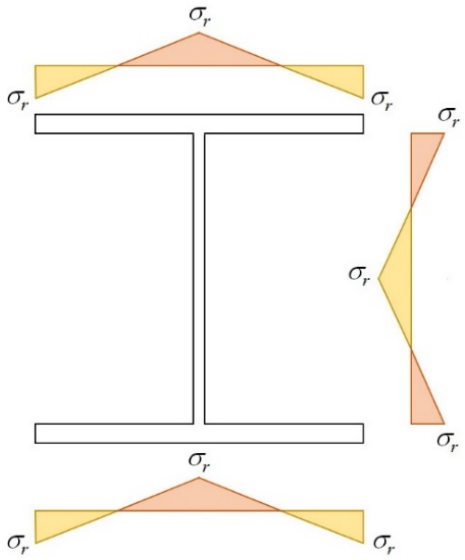

Fig. 3 ECCS residual stress pattern.

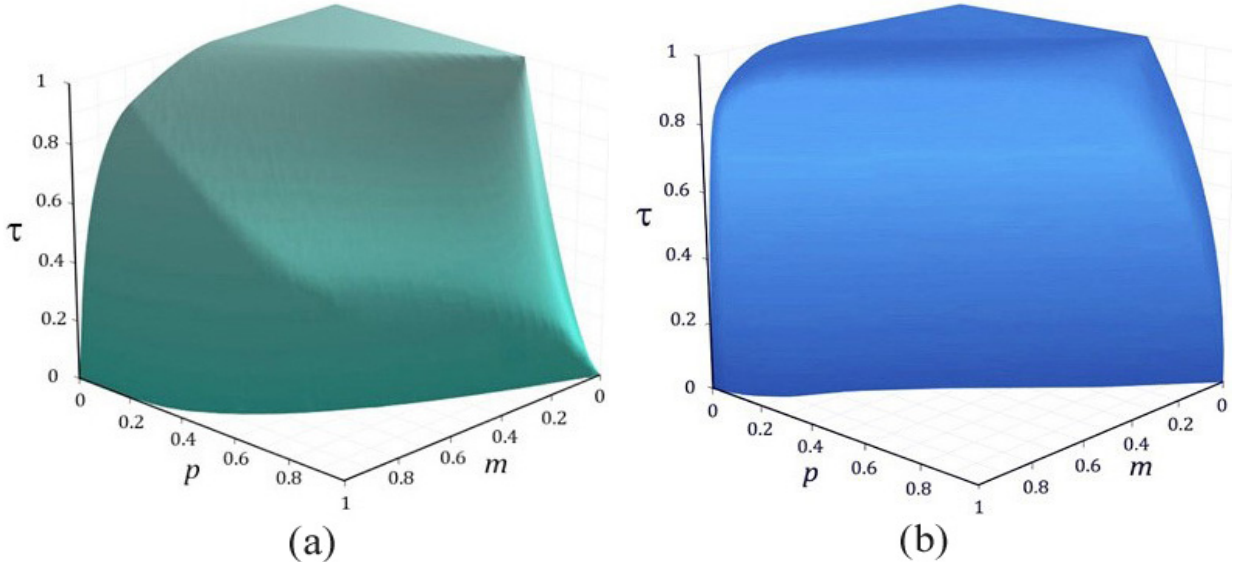

Fig. 4 *m-p-τ* surface plot of a W8x31 for (a) minor axis bending and (b) major axis bending.

$$m_0 = \frac{4 - [p(2+\lambda) - \lambda]^2}{2(2 + \lambda\lambda_o)} \quad when\ p \geq \frac{2\lambda_o + \lambda}{2 + \lambda} \tag{11}$$

The major axis bending moment m_0 at which $\tau = 0$ is given as

$$m_0 = 1 - \frac{p^2(2+\lambda)^2}{4\lambda_o + \lambda(4+\lambda)} \tag{12}$$

$$m_0 = \frac{(2+\lambda_1)^2 - [p(2+\lambda) - \lambda + \lambda_1]^2}{4 + \lambda_1(4+\lambda)} \quad when\ p \geq \frac{\lambda}{2+\lambda} \tag{13}$$

where $\lambda = A_w/A_f$, $\lambda_o = t_w/b_f$, $\lambda_1 = d_w/t_f$ [12]. A_w is the web area, A_f is the flange area, t_w is the web thickness, b_f is the flange width, d_w is the web depth, and t_f is the flange thickness.

Using a linear variation in stiffness between the elastic condition of $\tau = 1$ and the fully plastic condition of $\tau = 0$, the stiffness reduction τ for a given m and p condition is evaluated based on the m_1 and m_0 values from Eqs. (8) through (13).

$$\tau = \frac{m_0 - m}{m_0 - m_1} \tag{14}$$

$$\tau = \left(\frac{1-p}{c_r}\right)\left(1-\frac{m}{m_0}\right) \; when \; p \geq 1-c_r \quad (15)$$

The generalized material models in Fig. 5 have been shown to be an effective approximation of the *m-p-τ* surface plotsin Fig. 4 [12]. Frame behavior results using Eqs. (14) and (15) to model the stiffness reduction were found to be in close agreement with El-Zanaty et al. [13] benchmark frame in Attalla et al. [1], King et al. [14], and Ziemian and McGuire [2].

For the condition of reduced flexural stiffness EI_{ep} that varies over a yielded region L_{ep}, it is necessary to use an iterative procedure with increments of load to produce the moments as depicted in Fig. 6 [15]. The area expression in Eq. (4) is evaluated to accommodate the increments of moment and reduced stiffness over the elasto-plastic region as

$$A_{ep} = \int_0^{L_{ep}} \frac{\Delta M_{ep}^H(z)}{EI_{ep}(z)}\,dz \quad (16)$$

Since the load ΔH is a concentrated force in Fig. 1, the moment equation for $\Delta M_{ep}^H(z)$ is linear over the yielded region, and the moment increments vary between ΔM_i and ΔM_j in Fig. 6 according to the following relationship

$$\Delta M_{ep}^H(z) = \Delta M_i + \frac{(\Delta M_j - \Delta M_i)z}{L_{ep}} \quad (17)$$

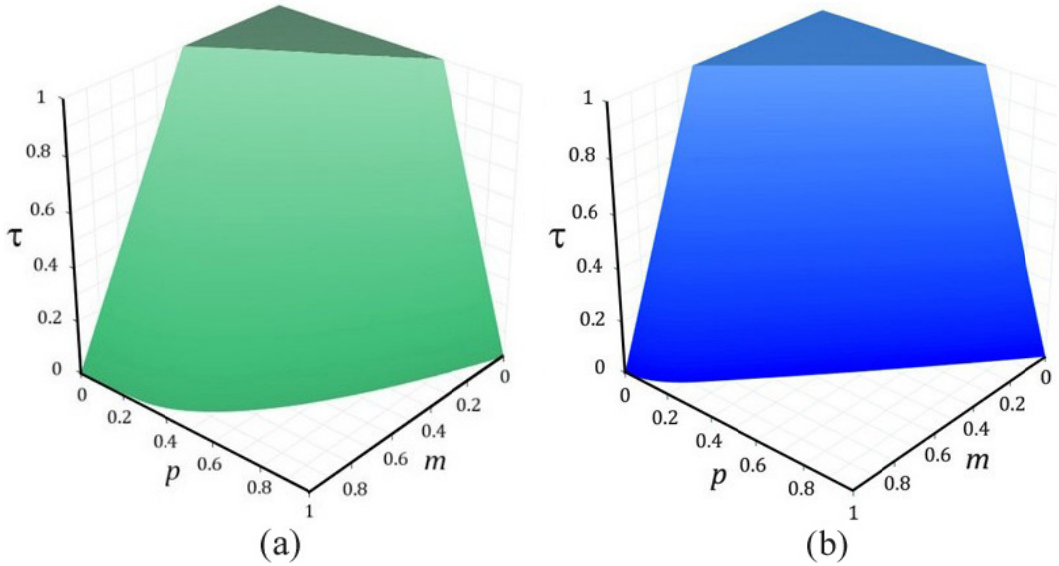

Fig. 5 Material model for (a) minor axis bending and (b) major axis bending.

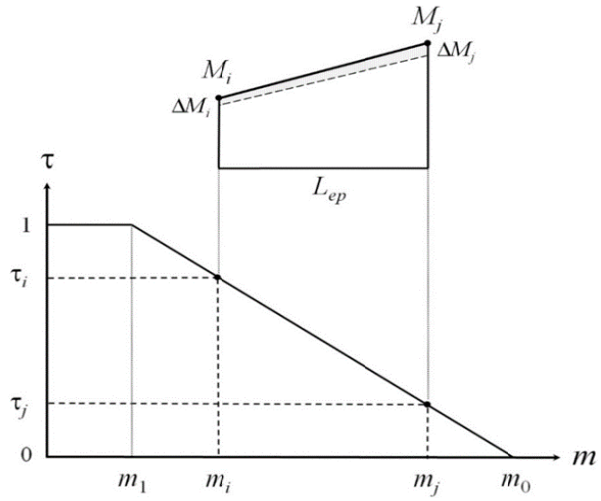

Fig. 6 Reduced stiffness over yielded region L_{ep} when $p < 1 - c_r$.

The denominator of Eq. (16) is evaluated using the member axial load $p(P/P_y)$ and the moments $m_i(M_i/M_p)$ and $m_j(M_j/M_p)$. The reduced stiffness $EI_{ep}(z)$ in Fig. 6 is written in terms of τ_i and τ_j as

$$EI_{ep}(z) = \tau(z)EI = \left[\tau_i + \frac{(\tau_j - \tau_i)z}{L_{ep}}\right]EI \quad (18)$$

where $\tau_i = (m_0 - m_i)/(m_0 - m_1)$
and $\tau_j = (m_0 - m_j)/(m_0 - m_1)$.

Substituting Eqs. (17) and (18) into Eq. (16), and evaluating the integral, yields the following closed-form expression for the area A_{ep} as depicted in Fig. 7.

$$A_{ep} = \left[1 - \left(\frac{\tau_i}{\tau_j - \tau_i} - \frac{\Delta M_i}{\Delta M_j - \Delta M_i}\right) ln\left(\frac{\tau_j}{\tau_i}\right)\right] \times \left(\frac{\Delta M_j - \Delta M_i}{\tau_j - \tau_i}\right)\frac{L_{ep}}{EI} \quad (19)$$

The centroid of this area is evaluated using the following expression

$$A_{ep}\bar{z}_{ep} = \int_0^{L_{ep}} \frac{\Delta M_{ep}^H(z)z}{EI_{ep}(z)}dz \quad (20)$$

Substituting Eqs. (17) and (18) into Eq. (20), the centroid $\bar{z}_{ep}$ as depicted in Fig. 7 is determined by dividing the integral solution by the area obtained from Eq. (19).

$$\bar{z}_{ep} = \left[\frac{\frac{1}{2}\left(\frac{\Delta M_j + \Delta M_i}{\Delta M_j - \Delta M_i}\right)}{1 - \left(\frac{\tau_i}{\tau_j - \tau_i} - \frac{\Delta M_i}{\Delta M_j - \Delta M_i}\right) ln\left(\frac{\tau_j}{\tau_i}\right)} - \frac{\tau_i}{\tau_j - \tau_i}\right] L_{ep} \quad (21)$$

3. Modeling First-Order, Inelastic Behavior

The first example will use the frame and loading condition in Fig. 1 to demonstrate the use of the equations to perform a first-order, inelastic analysis. The two columns are modeled as compact W8x31 W-Shape sections and the girder is modeled as a W10x60. All structural members are modeled as ASTM A992 steel [11] with material behavior as depicted in Fig. 5. Each member is oriented with major axis bending and length defined as $l/r_x = 31$. The load H in Fig. 1 is applied in ΔH increments using a simple-step procedure with $\Delta H = P_y/42{,}500$. The lateral displacement at point *c* is evaluated up to the maximum H value when frame instability initiates.

As depicted in Fig. 8a, the frame initially responds in an elastic manner with a constant EI_k^* in Eq. (4). For the W8x31 with $c_r = 0.3$ and $p = 0$, Eqs. (9) and (12) give $m_1 = 0.633$ and $m_0 = 1$. The response of the W10x60 remains elastic up to the maximum load condition. Until m_1 is reached in member *bc*, the increment of displacement at *c* is determined using

$$\delta_{cb} = A_{ab}\Delta\bar{M}_{ab}^Q + A_{bc}\Delta\bar{M}_{bc}^Q + A_{cd}\Delta\bar{M}_{cd}^Q \quad (22)$$

where the area and centroid values are determined using Table 1 for the areas depicted in Fig. 8a.

For the moments in Fig. 8b for which yielding occurs, the stiffness reduction $\tau = 2.725 - 2.725m$ is obtained from Eq. (14). After yielding initiates, the increment of displacement at *c* is determined using Eq. (4) as

$$\delta_{cb} = A_{aa'}\Delta\bar{M}_{aa'}^Q + A_{a'b}\Delta\bar{M}_{a'b}^Q + A_{bc}\Delta\bar{M}_{bc}^Q + A_{cd}\Delta\bar{M}_{cd}^Q \quad (23)$$

where $A_{a'b}$ and $\Delta\bar{M}_{a'b}^Q$ are evaluated using Eqs. (19) and (21), respectively. For the member *bc*, the curvature diagram is constant with $\Delta M_b = \Delta M_c$; thus $A_{bc}\Delta\bar{M}_{bc}^Q$ is evaluated as a rectangular area with reduced stiffness $\tau_b = \tau_c$. During this phase of the analysis, the numerical procedure accommodates an adaptive length for members aa' and $a'b$ using the m_1 moment condition to locate a'.

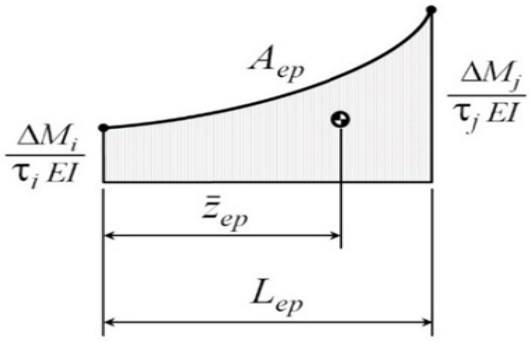

Fig. 7 Area and centroid of the curvature diagram in the elasto-plastic region.

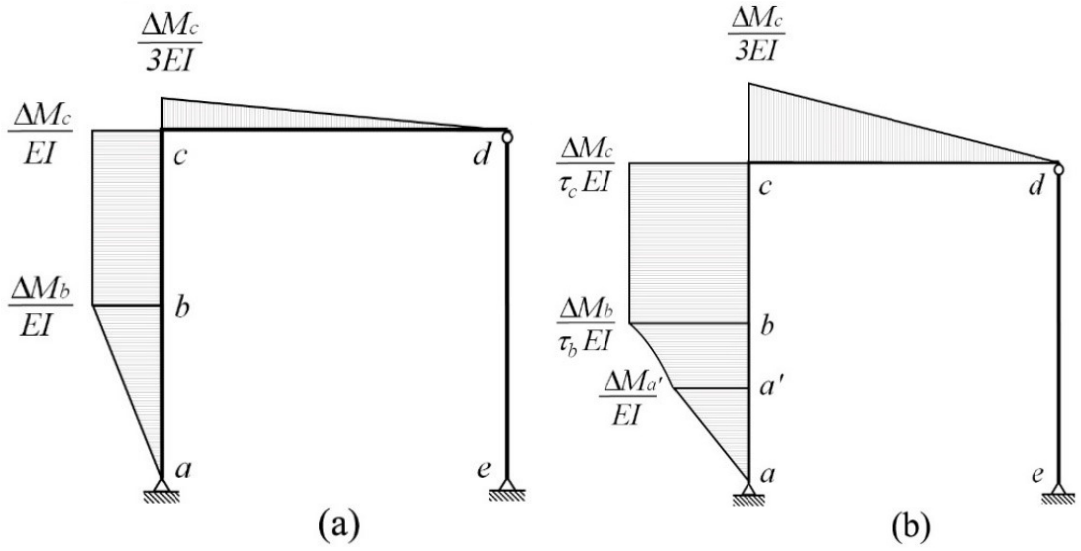

Fig. 8 Curvature diagrams during (a) elastic response and (b) inelastic response.

Table 1 Area and centroid formulas for curvature diagrams with constant stiffness.

Curvature Diagram	*Area* A	*Centroid* $\bar{z}$
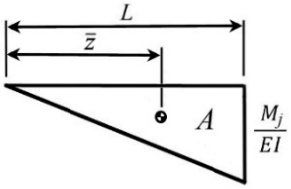	$\frac{M_j L}{2EI}$	$\frac{2L}{3}$
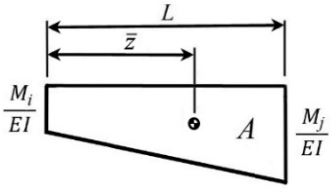	$\frac{(M_i + M_j)L}{2EI}$	$\frac{(M_i + 2M_j)L}{3(M_i + M_j)}$

The results from the virtual work method above were verified using the program MASTAN2 [8] with modifications to accommodate the material model defined by Eqs. (8) through (15). The closed-form stiffness matrix in Eq. (24) was developed by Ziemian and McGuire [2] and is part of the nonlinear material capabilities of MASTAN2. This stiffness matrix was developed using a linear variation in the tangent modulus over the element length and was chosen because the τ values from Eqs. (14) and (15) can be used directly for the a and b terms. The tangent modulus is defined as $E_{tm} = \tau E$. Since the normalized modulus is E_{tm}/E, then $a = \tau$ from the m and p conditions at the start of the element, and $b = \tau$ from the m and p conditions at the end of the element.

$$\frac{EI}{L}\begin{bmatrix} \frac{12}{L^2}\left(\frac{a+b}{2}\right) & -\frac{6}{L}\left(\frac{2a+b}{3}\right) & -\frac{12}{L^2}\left(\frac{a+b}{2}\right) & -\frac{6}{L}\left(\frac{a+2b}{3}\right) \\ & 4\left(\frac{3a+b}{4}\right) & \frac{6}{L}\left(\frac{2a+b}{3}\right) & 2\left(\frac{a+b}{2}\right) \\ & & \frac{12}{L^2}\left(\frac{a+b}{2}\right) & \frac{6}{L}\left(\frac{a+2b}{3}\right) \\ \textit{Sym.} & & & 4\left(\frac{a+3b}{4}\right) \end{bmatrix} \tag{24}$$

The frame was modeled using MASTAN2 with eight elements for the left column, and one element each for the girder and right column. As with the virtual work method, the lateral load was applied in $\Delta H = P_y/42{,}500$ increments using a simple-step procedure up to its maximum value of H. As depicted in Fig. 9, the frame initially responds in an elastic manner. At the end of this phase, the normalized load $HL/2M_p$ is 0.633 and the normalized displacement Δ/L is 0.0185 at point c. Beyond this point with additional increments of ΔH loading, inelastic response initiates with stiffness reduction from c to a'. It is during this phase that the results from the two analyses deviate slightly as indicated in Fig. 9. This is expected as the curvature over the length $a'b$ is modeled differently in each type of analysis method. The frame becomes unstable when the moment m_0 is reached in member bc. This occurs when the normalized load $HL/2M_p$ is 0.997 and the normalized displacement Δ/L is 0.0533at point c.

4. Modeling Second-Order, Inelastic Behavior

The first frame example demonstrated that modeling the inelastic material behavior of the left column in Fig. 8 using multiple elements with linear variation in stiffness in MASTAN2 provided almost identical results with that of the more detailed material model using Eqs. (19) and (21). In Fig. 10 the second-order effects that develop due to vertical loads V influence the curvature diagrams such that the assumed linear variation of moments over the member length (as given in Fig. 6) are no longer valid. For these two reasons, the curvature diagrams in the regions of the structure affected by second-order, inelastic response behavior are best approximated using multiple equally-spaced members with the virtual work method.

When the structure responds in an inelastic manner, Eq. (4) must be used with the vertical loads V fully applied throughout the analysis as the horizontal load H is applied incrementally. For each load increment ΔH, the area and centroid values of the curvature for each member are closely approximated using Table 1 with EI equal to the most recent EI_k^* value for each member.

The frame in Fig. 10 is modeled using the same structural properties as the first-order, inelastic frame example. The left side column is modeled using eight

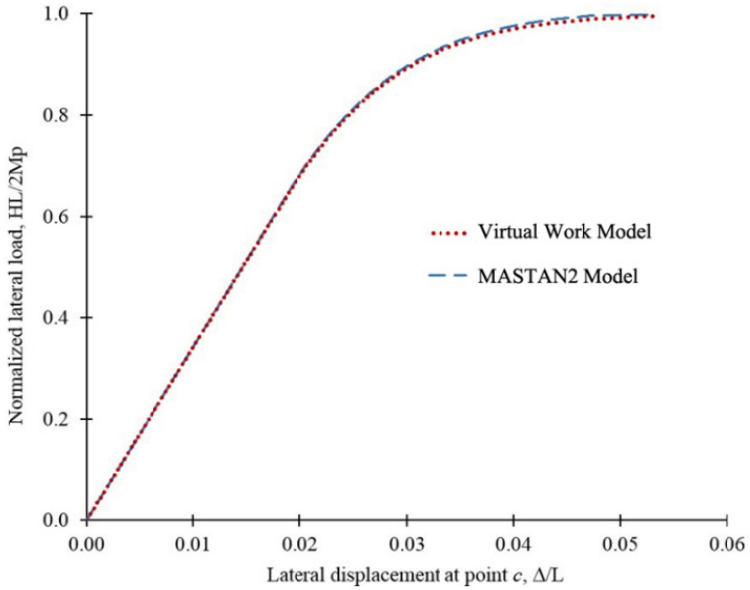

Fig. 9 First-order, inelastic load-displacement curves.

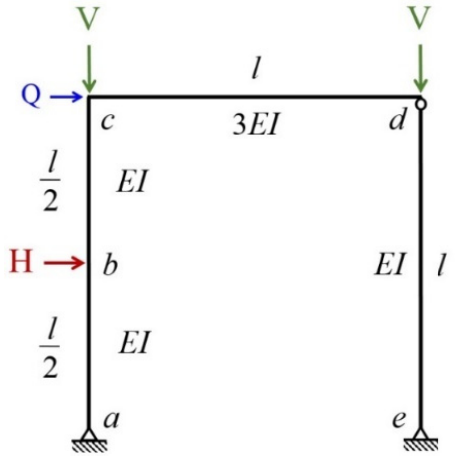

Fig. 10 Steel frame with loads H, V and Q.

equally-spaced members, and the girder and right column are modeled with only one member each since they remain elastic throughout the analysis. The vertical loads V are fully applied throughout the analysis and each are 20% of the column yield load P_y. The load H is applied in ΔH increments with ΔH = P_y/45,000. The lateral displacement at point c is evaluated up to the maximum H value when frame instability initiates.

The following two equations are used to evaluate the moment at any point j with a height z from the left support.

$$M_j = R_a^v \Delta_j + R_a^h z \qquad (25)$$

$$M_j = R_a^v \Delta_j + R_a^h z - r\Delta H\left(z - \frac{l}{2}\right) \; when \; z > \frac{l}{2} \qquad (26)$$

where r is the load increment number, and R_a^v and R_a^h are the vertical and horizontal reactions at point a, respectively.

$$R_a^v = V\left(1 - \frac{2\Delta_c}{l}\right) - \frac{r\Delta H}{2} \qquad (27)$$

$$R_a^h = V\left(\frac{\Delta_c}{l}\right)\left(1 + \frac{2\Delta_c}{l}\right) + r\Delta H\left(1 + \frac{\Delta_c}{2l}\right) \qquad (28)$$

For the W8x31 with c_r = 0.3 and p = 0.2, Eqs. (9) and (12) give m_1 = 0.451 and m_0 = 0.905. In Fig. 11 the frame initially responds in a second-order, elastic manner with a constant stiffness EI until m_1 is

reached at point *c*. This phase of response continues until load increment r = 805. At this point, the normalized load $HL/2M_p$ is 0.290 and the normalized displacement Δ/L is 0.0124 at point *c*.

As depicted in Fig. 12a, the frame then responds in a second-order, phase I inelastic manner with stiffness reduction initiating at point *c* and progressing down to point *b*. Phase I inelastic response ends at load increment r = 947 when the normalized load $HL/2M_p$ is 0.342 and normalized displacement Δ/L is 0.0147 at point *c*. Beyond this point with additional increments of ΔH loading, phase II inelastic response initiates with stiffness reduction progressing below point *b* as depicted in Fig. 12b. It is during this phase that the most significant nonlinear response is observed in Fig. 13. At load increment r = 1,328, the moment m_0 is reached at point *c* and the frame becomes unstable when the normalized load $HL/2M_p$ is 0.479 and the normalized displacement Δ/L is 0.0330 at point *c*.

The results from the method above were verified using the program MASTAN2. The frame was modeled using eight elements for the left column, and one element each for the girder and right column. As with the virtual work model, the lateral load was applied in increments using a simple-step procedure with $\Delta H = P_y/45{,}000$. The two curves in Fig. 13 indicate identical results. This is to be expected as each element of the MASTAN2 model with inelastic response was modeled using the same linear approximation for the variation in stiffness in Eq. (24). The only difference in the two analyses is that MASTAN2 terminates when the normalized load $HL/2M_p$ is 0.476 and the normalized displacement Δ/L is 0.0285 at point *c*. Comparing the two methods of analysis, the percent difference in the collapse load H is only 0.60%.

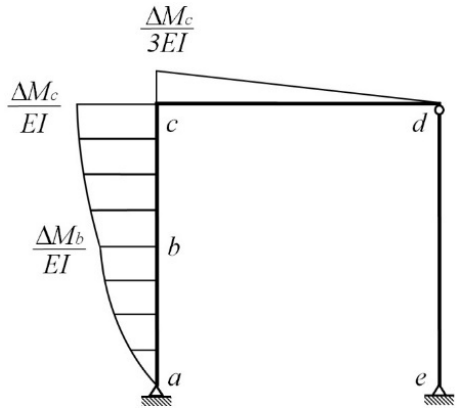

Fig. 11 Curvature diagram during second-order, elastic response.

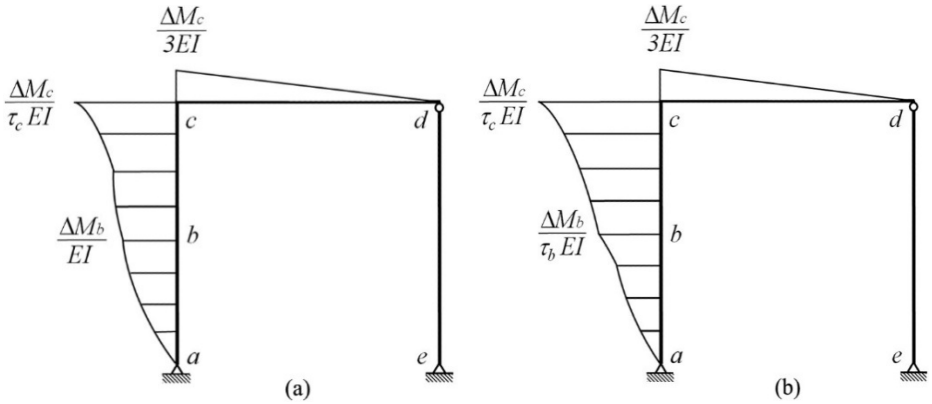

Fig. 12 Curvature diagrams during second-order: (a) phase I and (b) phase II inelastic response.

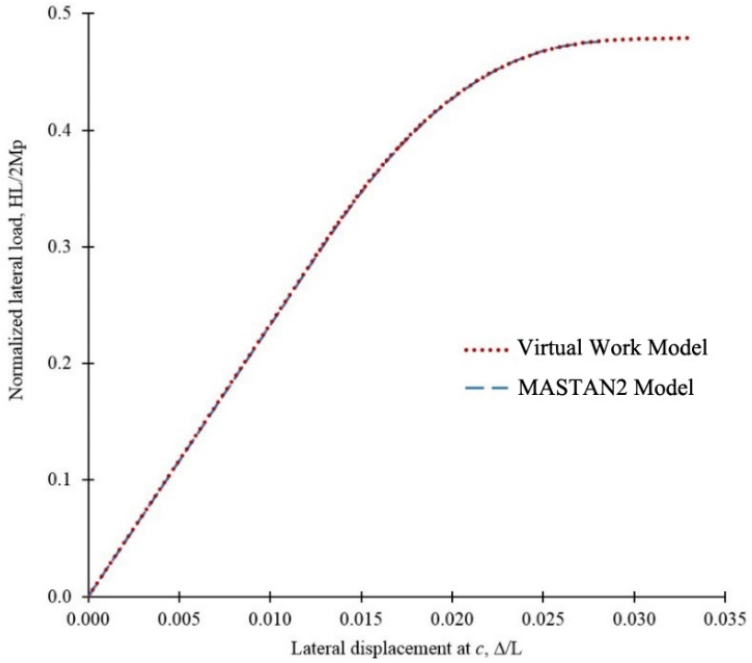

Fig. 13 Second-order, inelastic load-displacement curves.

5. Conclusions

Using the virtual work method, the response of steel frames due to inelastic material behavior and second-order effects was studied in detail. A detailed model of a W8x31 with 2,046 fiber elements was used to develop three-dimensional m-p-τ surface plots. A linear variation in reduced stiffness over the surface was used as a generalized material model between the initial yield and fully plastic conditions. The material model provides a straightforward and relatively easy to use means of conducting nonlinear analyses of planar steel frames with compact W-Shapes.

Although the paper used a W8x31with $c_r = 0.3$, the generalized material model can accommodate any W-Shape and assumed maximum value of residual stress. Compared with the direct stiffness method, or the more general finite element method, the paper demonstrates an alternative method of analysis when investigating nonlinear behavior of steel frames. The virtual work method explicitly uses incremental curvature diagram regions, and this provides the analyst with insights on when inelastic behavior initiates and on the progression of stiffness reduction throughout the structure up to the collapse condition.

Acknowledgments

The generosity of Prof. Ronald Ziemian in providing the MASTAN2 source code in order to input the generalized material model and verify the frame example results is gratefully acknowledged.

References

[1] Attalla, M. R., Deierlein, G. G., and McGuire, W. 1994. "Spread of Plasticity: Quasi-plastic-hinge Approach." *Journal of Structural Engineering* 120 (8): 2451-73.

[2] Ziemian, R. D., and McGuire, W. 2002. "Modified Tangent Modulus Approach, a Contribution to Plastic Hinge Analysis." *Journal of Structural Engineering* 128 (10): 1301-7.

[3] White, D. W, Liew, Y. J. R., and Chen, W. F. 1991. *Second-order Inelastic Analysis for Frame Design: A Report to SSRC Task Group 29 on Recent Research and the Perceived State-of-the-art.* Structural Engineering Report CE-STR-91-12, Department of Civil Engineering, Purdue University, West Lafayette.

[4] Ziemian, R. D., and Miller, A. R. 1997. "Inelastic Analysis and Design: Frames with Members in Minor-axis Bending." *Journal of Structural Engineering* 123 (2): 151-6.

[5] Zubydan, A. H. 2011. "Inelastic Second Order Analysis of Steel Frame Elements Flexed about Minor Axis." *Engineering Structures* 33: 1240-50.

[6] Kucukler, M., Gardner, L., and Macaroni, L. 2014. "A

Stiffness Reduction Method for the In-plane Design of Structural Steel Elements." *Engineering Structures* 73: 72-84.

[7] Kucukler, M., Gardner, L., and Macaroni, L. 2016. "Development and Assessment of a Practical Stiffness Reduction Method for the In-plane Design of Steel Frames." *Journal of Constructional Steel Research* 126: 187-200.

[8] Ziemian, R. D., and McGuire, W. 2015. MASTAN2. Ver. 3.5. www.mastan2.com.

[9] ECCS. 1984. *Ultimate Limit State Calculation of Sway Frames with Rigid Joints.* TC8 Publication No. 33. Brussels: European Convention for Constructional Steelwork.

[10] Rosson, B. T. 2016. "Elasto-plastic Stress States and Reduced Flexural Stiffness of Steel Beam-columns." In *Proceedings of the Annual Stability Conference*, Structural Stability Research Council, Orlando.

[11] AISC. 2011. *Steel Construction Manual*. Chicago: American Institute of Steel Construction.

[12] Rosson, B. T. 2017. "Major and Minor Axis Stiffness Reduction of Steel Beam-columns under Axial Compression and Tension Conditions." In *Proceedings of the Annual Stability Conference*, Structural Stability Research Council, San Antonio.

[13] El-Zanaty, M. H., Murray, D. W., and Bjorhovde, R. 1980. *Inelastic Behavior of Multistory Steel Frames.* Structural Engineering Report No. 83, University of Alberta, Edmonton.

[14] King, W. S., White, D. W., and Chen, W. F. 1992. "Second-order Inelastic Analysis Methods for Steel-frame Design." *Journal of Structural Engineering* 118 (2): 408-28.

[15] Rosson, B. T. 2018. *Introduction to Nonlinear Behavior of Structures*. Dubuque: Kendall Hunt Publishing.